frontiers | Frontiers in Materials

TYPE Original Research
PUBLISHED 28 July 2023
DOI 10.3389/fmats.2023.1238354

OPEN ACCESS

EDITED BY
Sheng Guo,
Chalmers University of Technology, Sweden

REVIEWED BY
Liuliu Han,
Max-Planck-Institut für Eisenforschung, Germany
Zhiqiang Fu,
South China University of Technology, China

*CORRESPONDENCE
Junfeng Zhao,
416zhaojunfeng@163.com

RECEIVED 11 June 2023
ACCEPTED 03 July 2023
PUBLISHED 28 July 2023

CITATION
Zhao J, Li X, Xie E, Mei H, Shen Y, Li K, Gong W and Wang L (2023), Study on the dissolution diffusion behavior of Al in Sn melt.
Front. Mater. 10:1238354.
doi: 10.3389/fmats.2023.1238354

Study on the dissolution diffusion behavior of Al in Sn melt

Junfeng Zhao[1,2,3,4]*, Xiaohui Li[2], En Xie[3], Haijuan Mei[1], Youqu Shen[1], Kai Li[1], Weiping Gong[1] and Liang Wang[4]

[1]Guangdong Provincial Key Laboratory of Electronic Functional Materials and Devices, Huizhou University, Huizhou, Guangdong, China, [2]Guangdong Tsing Impulse Science and Technology Co., Ltd., Foshan, China, [3]Huizhou Dejinchang Optoelectronics Technology Co., Ltd., Huizhou, Guangdong, China, [4]Shenzhen Zhixing New Materials Tech Co., Ltd., Shenzhen, China

The Al-Sn alloys with a large melting point difference and large density are widely used in sliding bearings in the aerospace and automobile industries. But the problem of insufficient alloying easily occurs during the preparation process due to the physical properties. This paper investigates the dissolution and diffusion behavior of Al in Sn Melt. The dissolution rates of Al in Sn melts at different temperatures were calculated. The research results show that the Al/Sn diffusion is dominated by the diffusion of Sn into Al, the Sn melt penetrate into the solid Al to form diffusion channel leading to the exfoliation and aggregation of the unmelted Al particles. Then, an electromagnetic field treatment technology was introduced to improve sufficient alloying by regulating the flow field of the metal melt. It can accelerate the diffusion and redistribution of elements at the Al/Sn solid-liquid interface, as well as change the dissolution mechanism of Al/Sn interface.

KEYWORDS

Al-Sn alloy, solid-liquid interface, dissolution, electromagnetic stirring, alloys with a large melting point difference

1 Introduction

The Al-Sn alloys are widely used in sliding bearings in the aerospace and automobile industries due to high wear resistance, conformability and compatibility (Lepper et al., 1997). Homogeneous microstructure of the alloys play a crucial role in mechanical properties developed (Marrocco et al., 2006). However, the system of Al-Sn has a wide miscibility gap in the liquid phase and does not form solid solution (Stuczynski, 1997), as well as has big density difference between the two components, these is a very sedimentary tendency in conventional casting processes leading to insufficient alloying (Pathak and Mohan, 2003). The preparation process of the alloy is closely related to its performance, and successful preparation is a necessary precondition for its excellent performance. Moreover, sufficient alloying is an important prerequisite for the successful preparation of the alloy (Li et al., 2021; Xu et al., 2021). There is a class of alloys with large melting point difference and large density difference, which are prone to insufficient alloying in the preparation due to the significant difference in physical properties between alloy components (Wu et al., 2020; Wang et al., 2022). Such alloys are typically represented by U-Nb (Sen-Britain and Nelson, 2022; Wang et al., 2022), Al-Sn (Liu et al., 2009), Cu-Bi (Chang et al., 1997; Palmer et al., 2019), Al-Bi (Silva et al., 2010), Ga-Bi (Kuczkowski et al., 2000), *etc.* The U-Nb alloy has excellent mechanical and corrosion resistance, which is widely used in the military industry(Xue et al., 2020). The Cu-Bi alloy is an ideal bearing material because of its remarkable anti-friction properties (Ruiz-Gómez et al., 2022). Due to the special metallurgical

characteristics of these alloys, insufficient alloying and serious segregation easily occur under ordinary traditional casting conditions (Liu et al., 2009). In order to fabricate these alloys with homogeneous microstructure, different preparing methods have been used, such as power metallurgy (Liu et al., 2008), physical vapor deposition (Perrone et al., 2002) and so on (Barna et al., 1993; Suryanarayana, 2001; Noskova et al., 2006). The preparation of high-quality alloys with large melting point difference and large density difference has always been the key and difficulty in the field of engineering materials (Noskova et al., 2006).

During past decades, electromagnetic stirring has been demonstrated that alloys with homogeneous microstructure can be easily obtained (Agrawal et al., 2017). The electromagnetic field has a good effect on regulating the flow field, however there are few studies on its application in the alloy dissolution process. The electromagnetic machining technology, a non-contact external field machining method with the utilization of the electromagnetic fields, provides a new way for controlling the alloy melt flow (Usui et al., 2006). The Lorentz force induced by the magnetic field is used to exert vibration or stirring force on the liquid metal to control its mass transfer, momentum transfer and heat transfer process (Räbiger et al., 2012; Zheng et al., 2015), and then affect the microstructure and properties of the material (Yasuda et al., 2006). The electrical body force induced by the electric field can destabilize the melt flow, resulting in significant perturbation inside the melt (Chang et al., 2011). The application of electromagnetic fields can reduce the formation energy and migration activation energy of vacancies, promote their diffusion, and increasing the concentration of vacancies. Therefore, in the alloying process, the electromagnetic field can play the role of "energy regulator" to accelerate the dissolution and diffusion.

To tackle the challenge of insufficient alloying during the preparation process of Al-Sn alloys with high melting points and significant density differences, this study aims to enhance the melt flow field by introducing electromagnetic fields during the alloying process. The primary objective is to accelerate the dissolution of high melting point elements.

2 Experimental procedures

The raw materials selected are industrial pure Al wires with a diameter of 4 mm and high-purity Sn ingot. Tables 1, 2 show the composition contents of pure Al wire and high-purity Sn ingot, respectively.

TABLE 1 Chemical composition of industrial pure Al wires.

Composition	Cu (%)	Fe (%)	Mg (%)	H (%)	Si (%)	O (%)	Al (%)
(wt%)	0.095	0.13	0.22	0.035	0.042	0.028	99.5

TABLE 2 Chemical composition of high-purity Sn ingots.

Composition	Mg (%)	H (%)	O (%)	Sn (%)	Others (%)
(wt%)	0.001	0.0018	0.0012	99.995	0.001

Figure 1 is a schematic diagram of Al-Sn alloy diffusion. The Al wire was put into the graphite crucible, and the crucible was placed on the platform of the tensile device in the furnace. The crucible containing the Sn raw material was moved to the middle of the furnace through the tensile device to make the melt temperature as uniform as possible. Then, the furnace was heated to the set temperature for different times. During the diffusion process of the Al wire, the electromagnetic stirring can be controlled by the switch. When the Al wire was immersed in the Sn melt to reach the set time, the crucible was taken out and the ingot was directly water-cooled, the dissolution characteristics were evaluated.

The diameter of the Al wire after dissolution was measured by a caliper, and the data was used to calculate the dissolved amount of the Al in the Sn melt. In order to investigate the interfacial phenomena under different states, the solid-liquid interface microstructure and morphology of the samples were observed by scanning electron microscope (SEM, Hitachi S8010). Reaction layers at the interface were identified using energy-dispersive spectrophotometric (EDS) analysis.

3 Results and discussion

3.1 Dissolution rates of Al in Sn melts at different temperatures

Figure 2 shows schematic diagram of dissolution of Al in Sn melt. Table 3 shows the diameter data of Al in Sn melt with different temperature. According to the phase diagram of Al-Sn, it can be seen that no intermetallic compound is formed between Al-Sn, which means that there is no reaction diffusion at the Al/Sn solid-liquid interface during the dissolution process, but only interdiffusion behavior (McAlister and Kahan, 1983).

The dissolution flux of Al wire in Sn melt can be expressed in J,

$$J = -\frac{m}{A} = -\left(\rho_{Al}\frac{dV}{dt}\right)/A \tag{1}$$

m is the dissolving mass rate of Al wire, A the diffusion interface area, ρ_{Al} the density of Al wire, V the volume of Al and t the time. The volume change dV of aluminum can be expressed as:

$$dV = 2\pi rldr \tag{2}$$

r is the radius of aluminum and l is the calculated length of aluminum. The dissolution flux of Al wire in Sn melt can be expressed as follows:

$$J = -\rho_{Al}dr/dt = -\rho_{Al}v \tag{3}$$

Combined with the data in Table 1, the dissolution flux of Al calculated at 450, 500, and 550 °C are 0.324, 0.504, and 0.905 ($g/m^2{\cdot}s$), respectively. The dissolution behavior of Al in Sn melt is based on the thermal activation, so the dissolution flux can be described by Arrhenius equation:

$$J = J_0 \exp(-Q/RT) \tag{4}$$

J_0 is dissolution-diffusion flux constant. Take the logarithm of both sides of Eq 4, we have

$$InJ = InJ_0 + (-Q/R) \bullet \left(\frac{1}{T}\right) \tag{5}$$

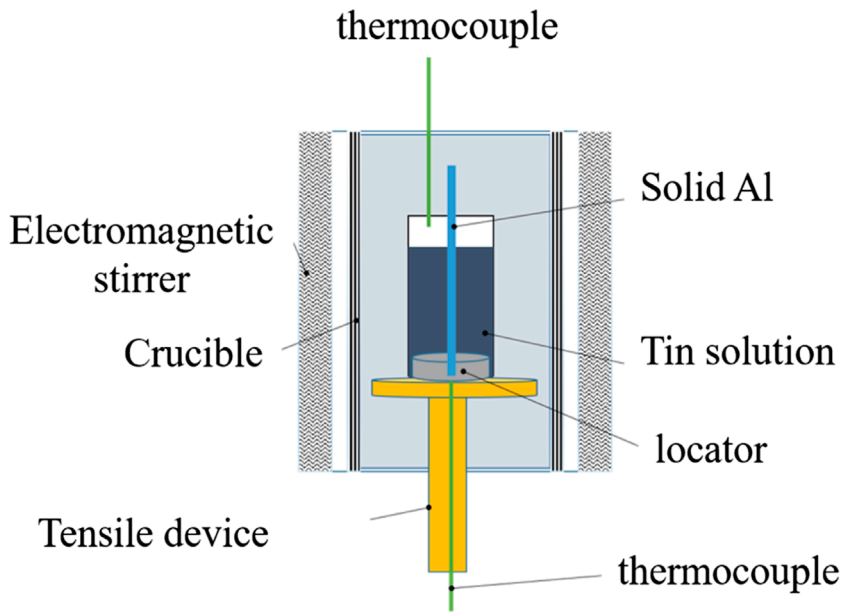

FIGURE 1
The schematic diagram of Al-Sn alloy dissolution.

FIGURE 2
Schematic diagram of dissolution of Al in Sn melt.

Using the dissolution flux data under different Sn melt temperature conditions, the ln$J$-1/T curve is ploted, as shown in Figure 3. After linear fitting, it can be seen that lnJ = 0.345 – 6082/T and the Q = 50.5657 kJ/mol

According to Eqs 3, 4, the relationship between the dissolution rate of Al in Sn melt and the temperature can be obtained as:

$$v = \frac{J_0}{\rho_{Al}} \exp\left(-\frac{Q}{RT}\right) \tag{6}$$

By substituting the density of Al and the calculated J_0 and Q values, the dissolution rate of Al in Sn melt can be expressed as:

$$v = 0.000523 \exp\left(-\frac{6082}{T}\right) \tag{7}$$

3.2 Analysis of al/Sn interface micromorphology and dissolution mechanism

Figure 4 shows the solid-liquid interface of the Al-Sn alloy after holding at 500 °C for different times. From the above test results, it can be seen that the Al wire gradually dissolves in the Sn liquid as the holding time increased. The Sn atoms dissolved in the Al surface layer under the action of interdiffusion. Since the melting point of embedded particles is strongly dependent on the nature of the particle/matrix interface (Allen et al., 1980), the melting will occurs when its melting point lower than the ambient temperature (Sn melt temperature). The liquid Sn/solid Al interface gradually moved to the side of the Al wire, and the diameter of the Al gradually decreased, which means that the Al wire gradually dissolved in the Sn melt. Once the Al wire starts to dissolve, the alloying reaction becomes self-propagating, as it is exothermic in nature, eliminating the need for additional heat supply (Baras and Politano, 2018). Figure 4B shows that the Sn liquid infiltrates along the surface defects of the Al wire to form a dissolution channel during this process. If the dissolution channel continues to extend and multiple dissolution channels cross each other, it will cause small Al particles in the surface of the Al wire to fall off.

Figure 5 shows the SEM and EDS images of Al and Sn at the solid-liquid interface at 500°C for 30 min. Interestingly, the Al/Sn interface is not a planar structure, but a dendritic structure with a certain orientation. From Figure 4B; Figure 5, small pieces of Al peel off from the solid-liquid interface during the dissolution process of the Al-Sn held at 500 °C for 30 min. After exfoliation, more small aluminum particles quickly moved to the surface of Sn melt and formed a large number of unmelted Al particles due to their density

TABLE 3 Diameter data of Al in Sn melt at different temperature in 10 min.

Temperature of Sn melt/°C	Diameter of Al before dissolution/mm	Thickness of Al dissolved layer/mm
450	4.0	0.072
500	4.0	0.112
550	4.0	0.201

[a]Date measured at thermal couple position.

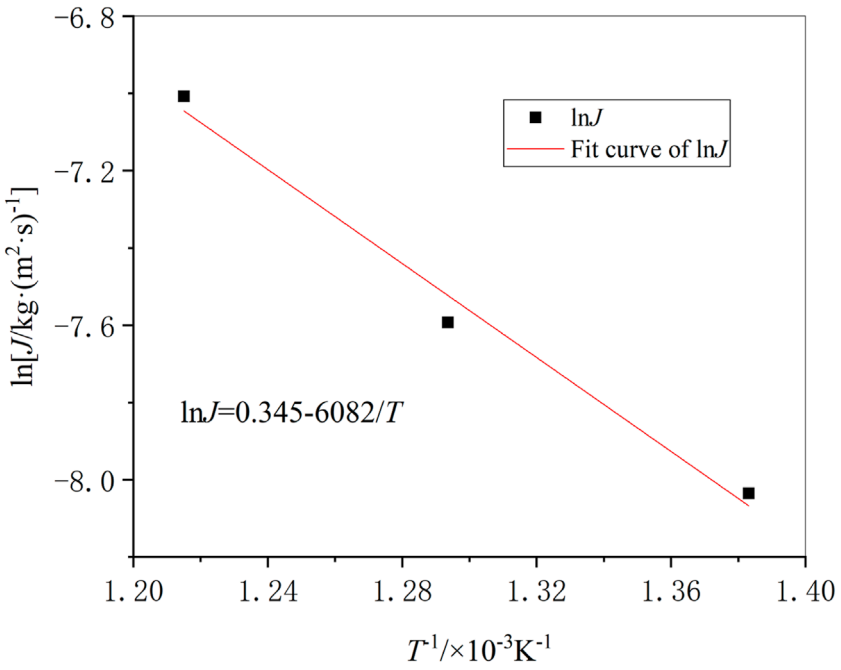

FIGURE 3
The relationship between ln*J* and 1/*T*.

was much lower than that of Sn melt. So only partially exfoliated small pieces of Al were observed in the images. Since the Sn melt on the surface is direct contact with the air, the falling Al partiles were easily oxidized and aggregated to form unmelted Al particle clusters, resulting in insufficient Al-Sn alloying.

Concerning the microstructure and morphology of the diffusion and dissolution behavior of Al/Sn, the dissolution mechanism of solid Al in Sn melt can be inferred as shown in Figure 6. During the initial stage of dissolution, the concentration gradient causes the Sn melt to selectively dissolve the Al present at grain boundaries or other defects, resulting in the formation of small pits on the surface of the Al. At this time, the diffusion behavior of Sn to Al dominates the Al/Sn interdiffusion. Then the Sn melt penetrates these small pits and continuously promotes the dissolution of Al to the interior of the solid Al. Due to the randomness of Al grain boundaries and internal defects, these dissolution channels gradually bend to form the aforementioned dendritic structure. A large number of unmelted Al are released after the dissolution channels are connected. Since the density of the Al particle is much lower than that of the Sn melt, the Al particles will float to the upper surface of the Sn melt to aggregate under the action of buoyancy, resulting in insufficient alloying during the preparation of the Al-Sn alloy.

3.3 Effect of electromagnetic stirring on the dissolution behavior of Al in Sn melt

In order to solve the problem of insufficient alloying, the dissolution behavior of Al in Sn melt under the action of electromagnetic fields was studied. The applied traveling wave magnetic field excitation current parameters are 100A, 20 Hz. Figure 7 shows the SEM micrographs of Al/Sn interface with traveling wave magnetic field at 500°C. Compared with the Al/Sn interface without electromagnetic stirring (Figure 5), the interface under electromagnetic stirring is relatively flat, and the dendritic structure grooves basically disappear. At the same time and temperature, the Al hardly dissolves in Sn melt in Figure 4, while the dissolution of Al in Sn melt has been basically completed in Figure 7D, which indicates that electromagnetic stirring can

10.3389/fmats.2023.1238354

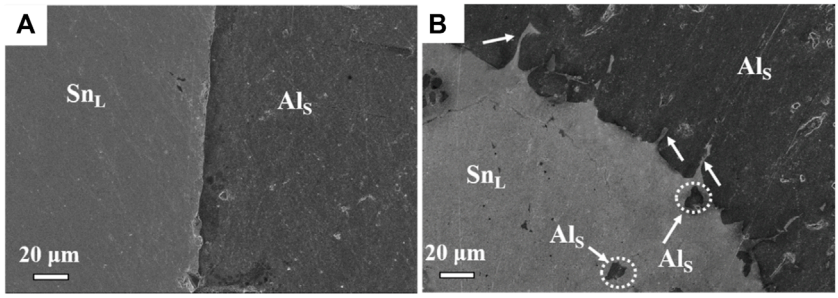

FIGURE 4
The solid-liquid interface of Al-Sn ingot held at 500°C **(A)** 10 min; **(B)** 30 min.

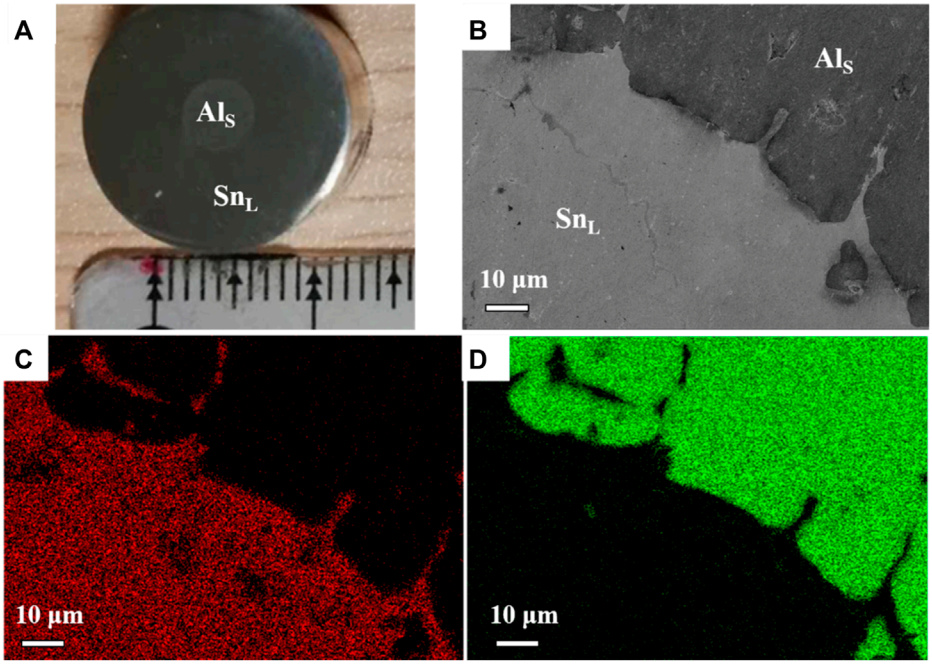

FIGURE 5
Al wire in Sn melt held at 500°C for 30 min **(A)**, the macrostructure of the Al/Sn; **(B)**, SEM image of the Al/Sn interface; **(C)**, the element Al in **(B)**; **(D)**, the element Sn in b.

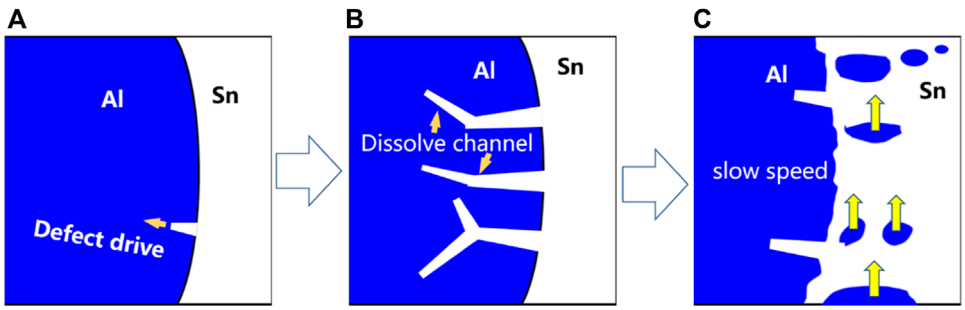

FIGURE 6
The Al/Sn dissolution model diagram without external field.

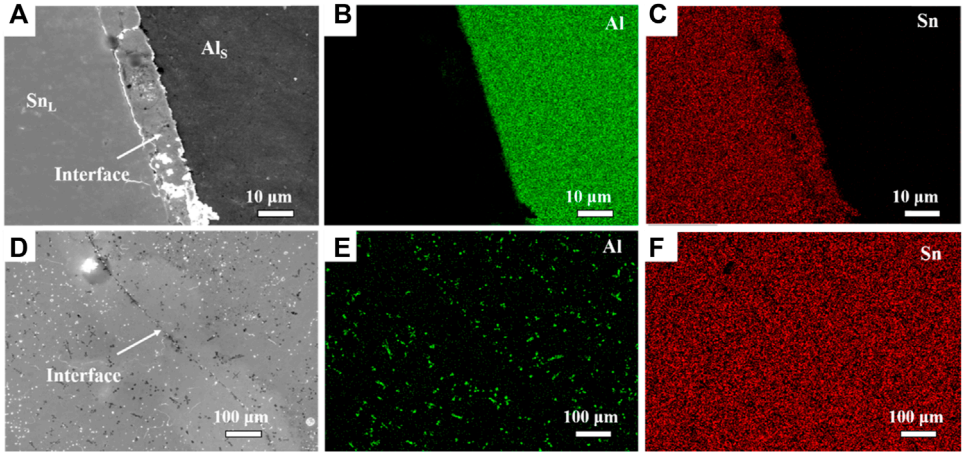

FIGURE 7
SEM micrographs of Al/Sn interface with traveling wave magnetic field at 500°C. **(A)** 20 min; **(B)** the element Al in a; **(C)** the element Sn in a **(D)** 30 min; **(E)** the element Al in d; **(F)** the element Sn in d.

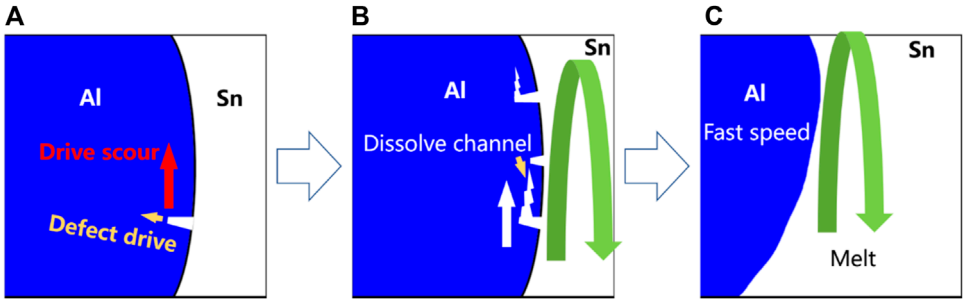

FIGURE 8
The model diagram of Al/Sn dissolution under the action of traveling wave magnetic field.

promote the dissolution of Al in Sn melt. The electromagnetic force induces vigorous convection, which enhances solute exchange at the interface, narrows the diffusion zone, and inhibits the formation of bulk structure. Under the action of the traveling wave magnetic field, the Sn melt forms a symmetrical eddy current. The movement of the flow field formed by the traveling wave magnetic field can accelerate the heat transfer in the melt, thereby weakening the temperature gradient. The model diagram of Al/Sn dissolution under the action of electromagnetic field is shown in Figure 8.

The Al wire is easily oxidized and a dense Al_2O_3 oxide film is formed on the surface (Zhao and Li, 2019). The oxide film hinders the diffusion of Al atoms and reduces the Al dissolution rate in the absence of a magnetic field. The implementation of an electromagnetic field can create a continuous scouring and impacting effect on the surface of the Al wire, which can cause the oxide film to break, crack or fall off. The fresh surface of the Al wire is more likely to inter-diffuse with Sn, which further accelerates the dissolution of the Al wire.

The concentration gradient of solute elements at the solid-liquid interface of the melt plays a significant role as a driving force for the dissolution process. In the absence of an external electromagnetic field, the inter-diffusion zone on the surface of the Al tends to be wide, and the concentration gradient is relatively small. As a result, the dissolution and diffusion rate is low because the small diffusion driving force limits the rate at which solute elements can dissolve and diffuse. When an external electromagnetic field is applied, the dissolved Al element at the solid-liquid interface is rapidly removed through forced convection. This leads to a reduction in the width of the inter-diffusion zone and an increase in the concentration gradient. Hence, as the diffusion driving force increases, the dissolution and diffusion rate also increase.

Through the above analysis, it can also be found that the high-speed flow of Sn melt is affected by the external electromagnetic field, which benefits the homogenization of the alloy melt. The uniform alloy structure can be obtained by the subsequent rapid solidification process. That is to say, the external electromagnetic field can improve sufficient alloying in the Al-Sn alloy.

4 Conclusion

1) The dissolution rate of Al in Sn melt can be described by the following relationship with the temperature of the Sn solution: $v = 0.000523\exp\left(-\frac{6082}{T}\right)(\mathrm{m/s})$
2) During the dissolution of Al in the Sn melt, the main diffusion process is the diffusion of Sn into Al. This leads to the creation of dissolution channels as the Sn melt permeates the solid Al, resulting in exfoliation and aggregation of unmelted Al particles.
3) Electromagnetic stirring can enhance the rate of Al dissolution in Sn melt and alter the dissolution mechanism of Al/Sn alloy. This acceleration facilitates effective alloying of alloys with a large melting point difference.

Data availability statement

The original contributions presented in the study are included in the article/Supplementary material, further inquiries can be directed to the corresponding author.

Author contributions

JZ designed the experiments and wrote the manuscript; XL revised the manuscript; EX provided materials and resources. All authors contributed to the article and approved the submitted version.

Funding

This study was financially supported by the Featured Innovation Project of General Colleges and Universities in Guangdong Province (2022KTSCX137) and the Scientific Research Startup Project for Doctors in Huizhou University (2021JB0061).

Conflict of interest

JZ and XL were employed by the Guangdong Tsing Impulse Science and Technology Co., Ltd. JZ and EX were employed by the Huizhou Dejinchang Optoelectronics Technology Co., Ltd. JZ and LW were employed by the Shenzhen Zhixing New Materials Tech Co., Ltd.

The remaining authors declare that the research was conducted in the absence of any commercial or financial relationships that could be construed as a potential conflict of interest.

Publisher's note

All claims expressed in this article are solely those of the authors and do not necessarily represent those of their affiliated organizations, or those of the publisher, the editors and the reviewers. Any product that may be evaluated in this article, or claim that may be made by its manufacturer, is not guaranteed or endorsed by the publisher.

References

Agrawal, S., Ghose, A., and Chakrabarty, I. (2017). Effect of rotary electromagnetic stirring during solidification of *in-situ* Al-TiB2 composites. *Mater. Des.* 113, 195–206. doi:10.1016/j.matdes.2016.10.007

Allen, G., Gile, W., and Jesser, W. (1980). The melting temperature of microcrystals embedded in a matrix. *Acta Metall.* 28 (12), 1695–1701. doi:10.1016/0001-6160(80)90022-x

Baras, F., and Politano, O. (2018). Epitaxial growth of the intermetallic compound NiAl on low-index Ni surfaces in Ni/Al reactive multilayer nanofoils. *Acta Mater.* 148, 133–146. doi:10.1016/j.actamat.2018.01.035

Barna, P., Barcza, G., Tóth, L., Vincze, G., Bergauer, A., and Bangert, H. (1993). Structural evolution in codeposited Al-Sn thin films. *Surf. Coatings Technol.* 57 (1), 7–11. doi:10.1016/0257-8972(93)90330-q

Chang, L., Straumal, B. B., Rabkin, E., Gust, W., and Sommer, F. (1997). The solidus line of the Cu-Bi phase diagram. *J. Phase Equilibria* 18 (2), 128–135. doi:10.1007/bf02665694

Chang, M.-H., Ruo, A. C., Chen, F., and Chang, S. T. (2011). The effect of Joule-heating-induced buoyancy on the electrohydrodynamic instability in a fluid layer with electrical conductivity gradient. *Int. J. heat mass Transf.* 54 (17-18), 3837–3845. doi:10.1016/j.ijheatmasstransfer.2011.04.045

Kuczkowski, A., Thomas, F., Schulz, S., and Nieger, M. (2000). Synthesis and X-ray crystal structures of novel Al– Bi and Ga– Bi compounds. *Organometallics* 19 (26), 5758–5762. doi:10.1021/om0007365

Lepper, K., James, M., Chashechkina, J., and Rigney, D. (1997). Sliding behavior of selected aluminum alloys. *Wear* 203, 46–56. doi:10.1016/s0043-1648(96)07475-3

Li, W., Xie, D., Zhang, Y., Gao, Y., and Liaw, P. K. (2021). Mechanical behavior of high-entropy alloys. *Prog. Mater. Sci.* 118, 100777. doi:10.1016/j.pmatsci.2021.100777

Liu, X., Zeng, M., Ma, Y., and Zhu, M. (2008). Wear behavior of Al–Sn alloys with different distribution of Sn dispersoids manipulated by mechanical alloying and sintering. *Wear* 265 (11), 1857–1863. doi:10.1016/j.wear.2008.04.050

Liu, X., Zeng, M., and Zhu, M. (2009). Melting behavior and the correlation of Sn distribution on hardness in a nanostructured Al–Sn alloy. *Mater. Sci. Eng. A* 506 (1-2), 1–7. doi:10.1016/j.msea.2008.12.054

Marrocco, T., Driver, L., Harris, S., and McCartney, D. (2006). Microstructure and properties of thermally sprayed Al-Sn-based alloys for plain bearing applications. *J. Therm. spray Technol.* 15 (4), 634–639. doi:10.1361/105996306x-147009

McAlister, A., and Kahan, D. (1983). The Al– Sn (aluminum-tin) system. *Bull. Alloy Phase Diagrams* 4 (4), 410–414. doi:10.1007/bf02868095

Noskova, N., Vil'danova, N. F., Filippov, Y. I., Churbaev, R. V., Pereturina, I. A., Korshunov, L. G., et al. (2006). Preparation, deformation, and failure of functional Al-Sn and Al-Sn-Pb nanocrystalline alloys. *Phys. Metals Metallogr.* 102 (6), 646–651. doi:10.1134/s0031918x06120131

Palmer, C., Tarazkar, M., Kristoffersen, H. H., Gelinas, J., Gordon, M. J., McFarland, E. W., et al. (2019). Methane pyrolysis with a molten Cu–Bi alloy catalyst. *Acs Catal.* 9 (9), 8337–8345. doi:10.1021/acscatal.9b01833

Pathak, J., and Mohan, S. (2003). Tribological behaviour of conventional Al-Sn and equivalent Al-Pb alloys under lubrication. *Bull. Mater. Sci.* 26 (3), 315–320. doi:10.1007/bf02707453

Perrone, A., Zocco, A., de Rosa, H., Zimmermann, R., and Bersani, M. (2002). Al–Sn thin films deposited by pulsed laser ablation. *Mater. Sci. Eng. C* 22 (2), 465–468. doi:10.1016/s0928-4931(02)00188-1

Räbiger, D., Leonhardt, M., Eckert, S., and Gerbeth, G. (2012). Flow control during solidification of SnPb-alloys using time-modulated AC magnetic fields. *IOP Conf. Ser. Mater. Sci. Eng.* 27, 012053. doi:10.1088/1757-899X/27/1/012053

Ruiz-Gómez, S., Fernández-González, C., Guedeja-Marrón, A., Serrano, A., González Barrio, M. Á., Varela, M., et al. (2022). Highly Bi-doped electrodeposited Cu nanowires for spintronics applications. *J. Magnetism Magnetic Mater.* 545, 168645. doi:10.1016/j.jmmm.2021.168645

Sen-Britain, S., and Nelson, A. J. (2022). Study of cluster ions produced from ToF-SIMS analysis of a U-6%Nb target. *Nucl. Instrum. Methods Phys. Res. Sect. B Beam Interact. Mater. Atoms* 515, 37–47. doi:10.1016/j.nimb.2022.01.010

Silva, A. P., Spinelli, J. E., Mangelinck-Noël, N., and Garcia, A. (2010). Microstructural development during transient directional solidification of hypermonotectic Al–Bi alloys. *Mater. Des.* 31 (10), 4584–4591. doi:10.1016/j.matdes.2010.05.046

Stuczynski, T. (1997). Metallurgical problems associated with the production of aluminium-tin alloys. *Mater. Des.* 18 (4-6), 369–372. doi:10.1016/s0261-3069(97)00078-2

Suryanarayana, C. (2001). Mechanical alloying and milling. *Prog. Mater. Sci.* 46 (1-2), 1–184. doi:10.1016/s0079-6425(99)00010-9

Usui, M., Iwai, K., and Asai, S. (2006). Crystal alignment of Sn–Pb alloy by controlled imposition of a static magnetic field and an alternating electric current during solidification. *ISIJ Int.* 46 (6), 859–863. doi:10.2355/isijinternational.46.859

Wang, X., Wang, W., Lu, C., Zhao, Y., Qiu, R., Shi, T., et al. (2022). Interface structure of (130) twin in the U-14.0 at % Nb alloy: An experimental and theoretical study. *Scr. Mater.* 209, 114417. doi:10.1016/j.scriptamat.2021.114417

Wu, Z., Zhang, H., Yang, D., Zou, J., Qin, K., Ban, C., et al. (2020). Electrochemical behaviour and discharge characteristics of an Al–Zn–In–Sn anode for Al-air batteries in an alkaline electrolyte. *J. Alloys Compd.* 837, 155599. doi:10.1016/j.jallcom.2020.155599

Xu, Y., Zhang, Z., Gao, Z., Bai, Y., Zhao, P., and Mao, W. (2021). Effect of main elements (Zn, Mg and Cu) on the microstructure, castability and mechanical properties of 7xxx series aluminum alloys with Zr and Sc. *Mater. Charact.* 182, 111559. doi:10.1016/j.matchar.2021.111559

Xue, S., Ling, M. X., Liu, Y. L., Kang, Q. Q., Huang, R. F., Zhang, Z. K., et al. (2020). The formation of the giant Huayangchuan U-Nb deposit associated with carbonatite in the Qingling Orogenic Belt. *Ore Geol. Rev.* 122, 103498. doi:10.1016/j.oregeorev.2020.103498

Yasuda, H., Ohnaka, I., Fujimoto, S., Takezawa, N., Tsuchiyama, A., Nakano, T., et al. (2006). Fabrication of aligned pores in aluminum by electrochemical dissolution of monotectic alloys solidified under a magnetic field. *Scr. Mater.* 54 (4), 527–532. doi:10.1016/j.scriptamat.2005.10.059

Zhao, J., and Li, Q. (2019). Study on interfacial phenomena in aluminum–aluminum bimetal fabricated by extrusion at different temperatures. *J. Mater. Eng. Perform.* 28 (2), 1122–1131. doi:10.1007/s11665-018-3800-1

Zheng, T., Zhong, Y., Lei, Z., Ren, W., Ren, Z., Debray, F., et al. (2015). Effects of high static magnetic field on distribution of solid particles in BiZn immiscible alloys with metastable miscibility gap. *J. Alloys Compd.* 623, 36–41. doi:10.1016/j.jallcom.2014.10.095